


Article

Systematic Investigation of Prelithiated SiO₂ Particles for High-Performance Anodes in Lithium-Ion Battery

Yuyao Han ¹, Xinyi Liu ² and Zhenda Lu ^{1,*} 

¹ National Laboratory of Solid State Microstructures, College of Engineering and Applied Sciences and Collaborative Innovation Center of Advanced Microstructures, Nanjing University, Nanjing 210093, China; y_han07@163.com

² Nanjing Foreign Language School, Nanjing 210008, China; Liuxinyi2019@hotmail.com

* Correspondence: luzhenda@nju.edu.cn

Received: 22 June 2018; Accepted: 24 July 2018; Published: 27 July 2018



Abstract: Prelithiation is an important strategy used to compensate for lithium loss during the formation of a solid electrolyte interface (SEI) layer and the other irreversible reactions at the first stage of electrochemical cycling. In this paper, we report a systematic study of thermal prelithiation of SiO₂ particles with different sizes (6 nm, 20 nm, 300 nm and 3 μm). All four lithiated anodes (Li_xSi/Li₂O composites) show improved performance over pristine SiO₂. More interestingly, lithiated product from micron-sized SiO₂ particle demonstrates optimum performance with a charge capacity of 1859 mAhg⁻¹ initially and maintains above 1300 mAhg⁻¹ for over 50 cycles.

Keywords: lithium-ion battery; prelithiation; silicon oxides; Coulombic efficiency; microparticle

1. Introduction

Next generation high-capacity electrode materials are needed to meet the demands of the explosion of electricity-fueled forms of transportation [1–3]. Graphite, the commercial anode material, cannot completely satisfy the requirements of electric vehicles due to its relatively low theoretical specific capacity. To overcome this problem, numerous researchers have focused on silicon-based anode materials because of its high theoretical specific capacity and relatively low charge/discharge voltage. Among them, silica (SiO₂), the main institutions of sand and quartz, is generally considered to be a promising candidate [4–7]. Silica is easier to prepare and is much more economical than silicon, while also stores a large quantity of lithium and has a relatively low potential platform. However, bulk-SiO₂ is generally conformed to be lithium inactive due to instinctive insulation [8–11]. Therefore, considerable efforts have been devoted to various nanostructures, such as hollow nano-spheres [12], nano-films [8,11], nano-cubes [13], nanotubes [14] and nano-belts [15].

There is no denying that nano-structures can facilitate the diffusion of electron and lithium ion effectively. However, nano-structuring also has its limitations. Its higher specific surface area consumes the more electrolyte to form solid electrolyte interface (SEI), which results in lower Coulombic efficiency (CE) and capacity fading [16]. In addition, nano-structured materials usually have a low tap density, leading to a low volumetric capacity and a thick electrode at high mass loading [16,17]. As a result, maintaining the electrical and ionic pathways during cycling is difficult. Furthermore, nano-structuring usually requires a multi-step and advanced preparation process, leading to a higher cost. More seriously, silica can form a great deal of irreversible lithium silicates and Li₂O during the first lithiation cycle. This process consumes an excess amount of cathode materials [6–8,13,18,19], which significantly reduces the total energy density of full-cells, thereby preventing their practical applications. In order to tackle this issue, researchers have proposed prelithiation of the electrode material, which directly compensates for the irreversible loss of lithium during the first cycle [20–37]. For example, Tarascon's

group developed an electrochemical lithiation method to preload lithium in the Si and SiO₂ materials, which required the fabrication of a temporary cell and an inert atmosphere [35]. Recently, Cui's group developed thermal alloying silicon nanoparticles with molten lithium metal to obtain crystalline Li_xSi with good crystallinity and acceptable dry stability [31,32].

Here, we applied the thermal alloying method to the silica particles, achieved the prelithiated composites (Li_xSi/Li₂O), and finally studied their electrochemical properties. Such composites have multiple advantages: (1) prelithiation effectively improves the electrical conductivity of silica, making it easier to function as an anode with high capacity and cycle stability; (2) Li_xSi/Li₂O composites can address the low initial Coulombic efficiency (ICE) issue of Si-based anodes, which is a huge challenge for practical application; (3) Li_xSi/Li₂O composites alloy can serve as a promising anode containing lithium to pair with high-capacity lithium-free cathodes such as S for next-generation lithium-ion batteries. We have chosen different SiO₂ particles with different sizes (6 nm, 20 nm, 300 nm and 3 μm), and systematically studied their electrochemical performance. All prelithiated Li_xSi/Li₂O composites exhibit better performance than that of pristine SiO₂ particles. More interestingly, prelithiated composite from SiO₂ microparticle shows the best cycling stability, achieving a delithiation initial capacity of 1859 mAhg⁻¹ and keeping above 1300 mAhg⁻¹ after 50 cycles.

2. Materials and Methods

2.1. Synthesis of Li_xSi/Li₂O Composites

SiO₂ powders (about 6 nm, 20 nm, 300 nm, and 3 μm) were first dried under vacuum for 24 h to remove trapped water. Typically, the variously sized SiO₂ particles (200 mg) were mixed with Li metal (196 mg) in a tantalum crucible. Then, the mixtures were heated at 200 °C while they were mechanically stirred inside the tantalum crucible at 400 rpm for at least 6 h in a glove box (Ar atmosphere, O₂ level < 1.2 ppm, and H₂O level < 0.1 ppm, respectively). The powder turned to black during the reaction. The products were denoted as Li_xSi/Li₂O-1, Li_xSi/Li₂O-2, Li_xSi/Li₂O-3 and Li_xSi/Li₂O-4, corresponding to the different pristine SiO₂ particle sizes (6 nm, 20 nm, 300 nm, and 3 μm).

2.2. Morphological and Structural Characterizations

The crystal structures of the products were identified by X-ray diffractometer (XRD, Ultima III, Rigaku, Tokyo, Japan) using Kα radiation (40 Kv, 40 mA). The structure and morphology details of the products were observed by field-emission scanning electron microscopy (FESEM, Ultra 55, Zeiss, Germany) and transmission electron microscopy (TEM, Tecnai G² F20 X-TWIN, FEI). The particle size and size distributions were examined by Dynamic Light Scattering (DLS, Zetasizer Nano-ZS90, Malvern, UK).

2.3. Electrochemical Measurements

The electrochemical properties were carried out using LIR 2032-type coin cells. The active material was mixed with binder acetylene black and carboxymethyl cellulose (CMC) (weight ratio of 65:20:15) in tetrahydrofuran (THF) to form a slurry. Then, the slurry was uniformly spin-coated on copper foils. The mass loading of the slurry on each copper foil (12 mm) is about 0.3–3.5 mg. The electrodes were assembled in an Ar-filled glove box using lithium foil as the counter electrode and a Celgard 2300 film as the separator. An electrolyte solution consisting of 1 M LiPF₆ dissolved in ethylene (EC)/dimethyl carbonate (DMC) (1:1 by volume) was used to assemble the coin cells. Galvanostatic charge-discharge measurements were tested between 0.01 and 1.0 V at a rate of 0.05 C on the cell tester (LAND CT2001A, Wuhan, China). Cyclic voltammetry (CV) was conducted on an electrochemical workstation (Bio-logic VMP3) at a scan rate of 0.1 mVs⁻¹ in a potential range from 0.01 to 3.0 V. Electrochemical impedance spectroscopy (EIS) measurements were carried out on the same electrochemical workstation with

frequencies ranging from 100 kHz to 10 MHz, with an alternating voltage of 5 mV. All electrochemical measurements were carried out at room temperature.

3. Results and Discussion

To systematically study the effect of particle size, we selected different sizes of SiO₂ particles. As shown in Figure 1, the morphology and size distributions of particles were characterized by TEM, SEM and DLS measurement. Figure 1a–d show the morphology of pristine SiO₂ particles with different sizes from 6 nm to 3 μm. The TEM (Figure 1a,b) and SEM (Figure 1c,d) images clearly demonstrate all the silica particles have the spherical structures and uniform size. The size statistics by DLS further confirm that SiO₂ particles have a quite narrow size distribution (Figure 1e,h).

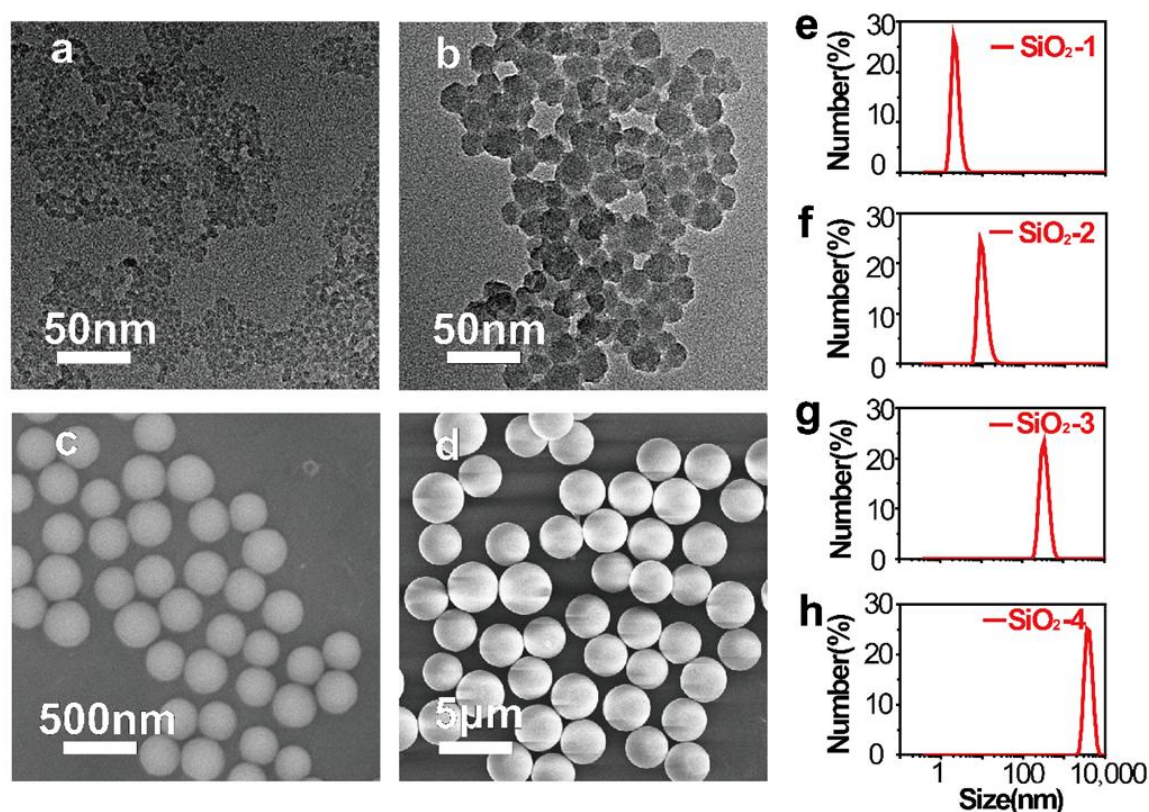


Figure 1. (a,b) TEM images of SiO₂-1 (6 nm) and SiO₂-2 (20 nm); (c,d) SEM images of SiO₂-3 (300 nm) and SiO₂-4 (3 μm); (e–h) The corresponding DLS analysis of the samples.

The SiO₂ particles with different sizes were alloyed with molten Li metal under Ar atmosphere to form Li_xSi/Li₂O NPs, as schemed in Figure 2a. The powder color changes from white to black within ten minutes, indicating the formation of Li_xSi alloy. SEM and TEM images (Figure 2b–e) demonstrate the morphology of as-prepared Li_xSi/Li₂O composites. After prelithiation, the surface of SiO₂ particles becomes rougher due to the coverage of oxide layer and volume expansion. Moreover, the images show that they have similar morphology despite being derived from variously sized SiO₂ particles. It is found that although the pristine SiO₂ particles varied from 6 nm to 3 μm, the over-all sizes of as-lithiated samples are all around several micrometers, which can be clearly seen from the enlarged SEM images in the insets. This can be attributed to the smaller particles undergo more severe aggregation during SiO₂ lithiation. As a result, Nanoparticles trend to aggregate into microparticles, while micro- or submicro-ones prefer to retain their size in the lithiation process. Figure 3a shows the XRD patterns of prelithiated SiO₂ particles. A home-made sealed sample holder was used to avoid exposing the products to the air. The diffraction peaks of Li₂O and Li₂₁Si₅ are shown in the Figure 3a,

demonstrating the formation of Li_2O (PDF# 04-001-893) and $\text{Li}_{21}\text{Si}_5$ (PDF# 00-018-747) phases. It has been reported that $\text{Li}_{21}\text{Si}_5$ is the most thermally stable phase among the crystalline lithium silicates [21]. The XRD patterns of the four $\text{Li}_x\text{Si}/\text{Li}_2\text{O}$ composites are similar, indicating that pristine particle size does not have a big effect on the formation of crystalline $\text{Li}_{21}\text{Si}_5$. As calculated by the Scherrer equation, the crystalline sizes of the four composites are 28.2, 29.3, 31.9 and 37.5 nm, indicating that the SiO_2 microparticles produce relatively large $\text{Li}_{21}\text{Si}_5$ domains.

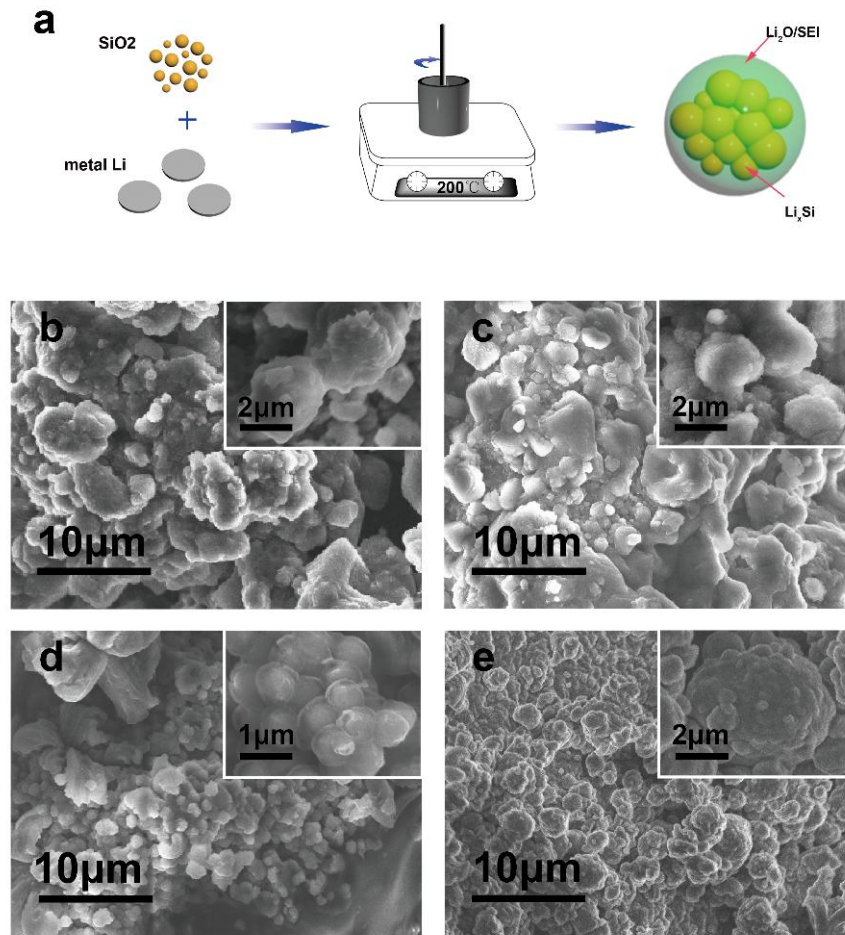


Figure 2. (a) Schematic of the thermal-alloying process of the SiO_2 with lithium metal; (b–e) SEM images of $\text{Li}_x\text{Si}/\text{Li}_2\text{O}$ -1, $\text{Li}_x\text{Si}/\text{Li}_2\text{O}$ -2, $\text{Li}_x\text{Si}/\text{Li}_2\text{O}$ -3, and $\text{Li}_x\text{Si}/\text{Li}_2\text{O}$ -4, respectively.

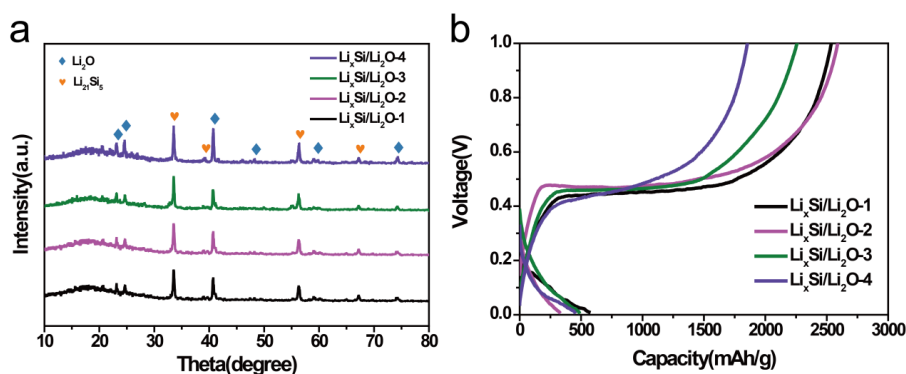


Figure 3. (a) XRD patterns of the four prelithiated composites; (b) The corresponding galvanostatic charge/discharge profiles of the $\text{Li}_x\text{Si}/\text{Li}_2\text{O}$ samples at the first cycle.

To invest the electrochemical behavior of the prelithiated products, half cells were fabricated with Li metal as a counter electrode. Figure 3b shows the charging/discharging profiles of $\text{Li}_x\text{Si}/\text{Li}_2\text{O}$ electrodes. The open-circuit voltage (OCV) of the half cells is around 0.35 V, which is significantly lower than ~ 2.0 V of the SiO_2/Li cell (SI, Figure S1). This proves that most SiO_2 particles were well lithiated. All of the lithiated SiO_2 electrodes exhibit the similar potential plateaus around 0.45 V, indicating the same active materials (Li_xSi) of the electrodes and their high crystallinity, consistent with the XRD results. The prelithiation capacities of the SiO_2 particles are 1972, 2267, 1776, and 1412 mAhg^{-1} , which are listed in Table 1. Here, the prelithiation capacity is determined by subtracting the lithiation capacity from the delithiation capacity at the first cycle. The thermal lithiation can effectively compensate for the huge irreversible lithium loss during the first cycles via the formation of lithium silicates and Li_2O . The cyclic voltammetry (CV) tests are conducted for both the pristine and prelithiated SiO_2 half cells for 3 consecutive cycles between 3.0 V and 0.01 V at a scan rate of 0.05 mVs^{-1} (Figure 4). The pristine SiO_2 electrode exhibits cathodic peaks above 1.0 V corresponding to the irreversible electrochemical reactions between the SiO_2 and Li, which disappears in the subsequent cycles. The cathodic peak below 0.2 V can be ascribed to the lithiation process of silicon. The electrochemical equations can be expressed as followed:

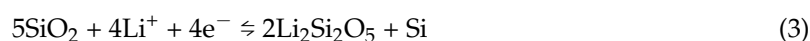
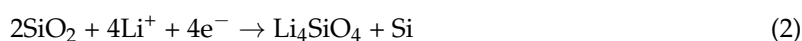
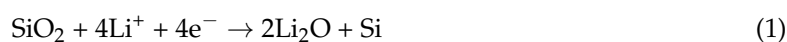


Table 1. Cycling performance for $\text{Li}_x\text{Si}/\text{Li}_2\text{O}$ electrodes.

Electrode	1st Delithiation Capacity/ mAhg^{-1}	Prelithiated Capacity/ mAhg^{-1}	25th Delithiation Capacity/ mAhg^{-1}	50th Delithiation Capacity/ mAhg^{-1}
$\text{Li}_x\text{Si}/\text{Li}_2\text{O}$ -1	2537	1972	795	673
$\text{Li}_x\text{Si}/\text{Li}_2\text{O}$ -2	2590	2267	900	913
$\text{Li}_x\text{Si}/\text{Li}_2\text{O}$ -3	2259	1776	1135	870
$\text{Li}_x\text{Si}/\text{Li}_2\text{O}$ -4	1859	1412	1510	1323

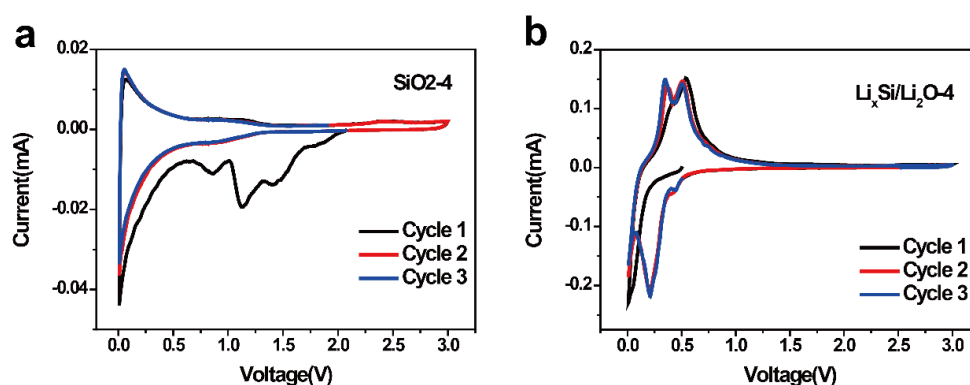


Figure 4. Cycling voltammetry measurement of SiO_2 electrodes before (a) and after (b) prelithiation.

For the $\text{Li}_x\text{Si}/\text{Li}_2\text{O}$ -4 anode, the corresponding peak of silicon lithiation is very pronounced. The cathodic peak at 0.5 V at the first cycle confirms the formation of highly crystalline Li_xSi . Two distinct anodic peaks at about 0.34 and 0.51 V during the second and third cycle agree with the characteristic peaks of delithiation process from amorphous Li_xSi to Si. The electrochemical equation can be expressed as followed:



The corresponding Nyquist plots measured at the first cycle are illustrated in supplement information (SI, Figure S2). $\text{Li}_x\text{Si}/\text{Li}_2\text{O}$ -4 anode demonstrated a smaller semicircle than the corresponding SiO_2 anode, indicating a lower charge transfer resistance (R_{ct}). It is clear that the prelithiated sample provides a fast electron transport pathway between the Li_xSi domains in the microparticles.

The cycling performance of prelithiated SiO_2 composites is shown in Figure 5a and listed in Table 1. The $\text{Li}_x\text{Si}/\text{Li}_2\text{O}$ composites deliver a first delithiation capacity of around 2000 mAhg^{-1} at $C/20$, with a corresponding Coulombic efficiency (CE) that is above 90% at initial cycles (Figure 5a and Figure S3). Very interestingly, the $\text{Li}_x\text{Si}/\text{Li}_2\text{O}$ -4 anode, prepared from micron-sized silica, has the best cycling stability among the four samples. It is able to maintain a stabilized reversible capacity of around 1300 mAhg^{-1} with acceptably small decay ($\sim 71\%$ capacity retention) after prolonged 50 cycles. The longer cycling performance is shown in supporting information, remaining around 800 mAhg^{-1} after 500 cycles. (Figure S4). The rate performance of $\text{Li}_x\text{Si}/\text{Li}_2\text{O}$ -4 anode was shown in Figure 5b. It yields a reversible capacity of over 1500 mAhg^{-1} at 0.05 C , around 1200 mAhg^{-1} at 0.1 C and 800 mAhg^{-1} at 0.2 C . At a high rate of as high as 1 C , the capacity is as low as 100 mAhg^{-1} . However, when the current rate reversed to 0.05 C , a high specific capacity have been recovered.

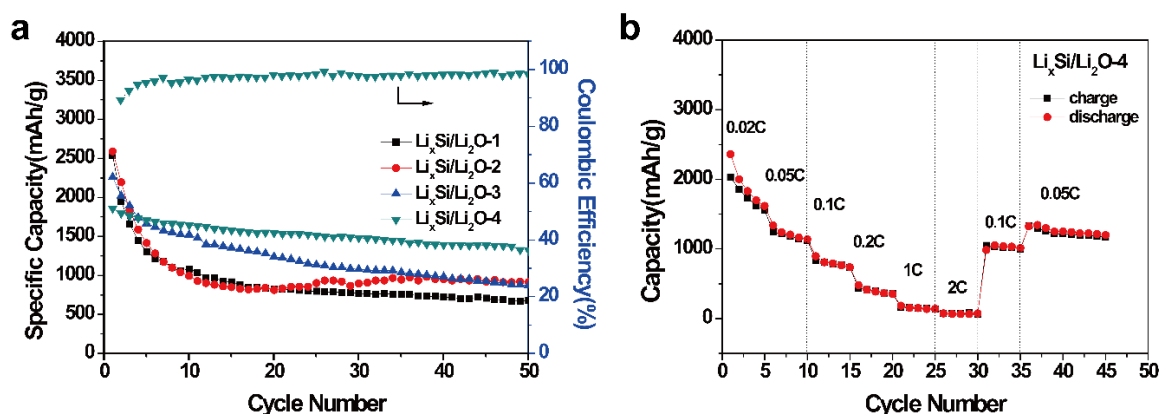


Figure 5. (a) Cycling performance of four $\text{Li}_x\text{Si}/\text{Li}_2\text{O}$ samples at $C/20$ ($1\text{C} = 1.96 \text{ A g}^{-1} \text{ Li}_x\text{Si}$, the capacity is based on the total mass of Li_xSi in the electrode). The green line is the Coulombic efficiency of $\text{Li}_x\text{Si}/\text{Li}_2\text{O}$ -4 composite; (b) Rate stability of $\text{Li}_x\text{Si}/\text{Li}_2\text{O}$ -4 composite.

As schemed in Figure 6, Li_xSi nano-domains are homogeneously dispersed in robust Li_2O matrix after the thermal prelithiation. For nano-sized SiO_2 particles, the Li_xSi domain is small and each domain is covered by a Li_2O layer. This Li_2O layer, formed by trace air oxidization of surface Li_xSi , is electrical insulating, which hinders the electrical conductivity between the $\text{Li}_x\text{Si}/\text{Si}$ nano-domains. After many electrochemical cycles, the electrical contact becomes even worse due to the SEI formation on these small domains. While for micron-sized particles, the Li_xSi domains are relatively large. In addition, oxidized Li_2O surface layer is mainly wrapped out of the whole microparticle, leaving Li_xSi domains contacting with each other inside the particle. The Li_2O outer layer can spatially limit the direct SEI formation on $\text{Li}_x\text{Si}/\text{Si}$ cores during the cycling. As a result, the $\text{Li}_x\text{Si}/\text{Li}_2\text{O}$ from SiO_2 microparticles can achieve enhanced cycling stability in half cells. Therefore, SiO_2 microparticle should be a very promising anode material, considering its low cost and the high cycling stability.

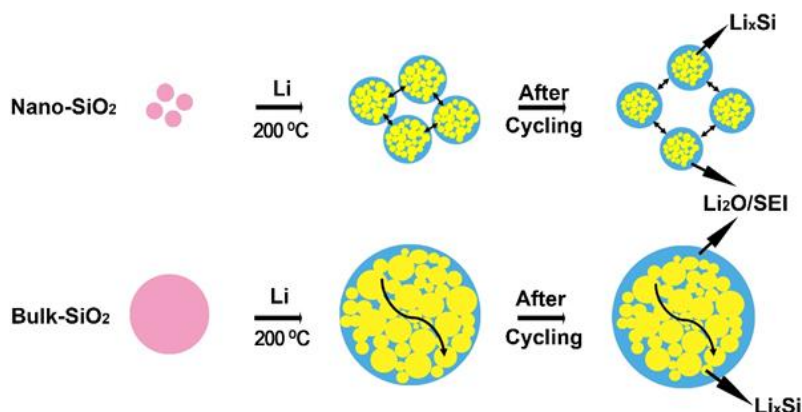


Figure 6. Schematic Illustration of the thermal prelithiation and electrochemical cycling of nano- and micron-sized SiO_2 particles.

4. Conclusions

In conclusion, this study explores the potential of using prelithiated SiO_2 particles as anode materials for high-capacity batteries. We systematically investigated SiO_2 particles with different sizes varying from 6 nm to 3 μm . All prelithiated composites exhibit better performance than that of untreated SiO_2 . The nano-particle, which is often thought to be more competitive in battery performance, however, lost its superiority after prelithiation. Contrary to our expectations, the micron-sized SiO_2 particle demonstrates more stable cycling performance, delivering a prelithiation capacity of 1412 mAhg^{-1} and a reversible specific capacity over 1300 mAhg^{-1} after 50 cycles. Considering the encouraging battery performance displayed, together with its abundance and low-cost, SiO_2 microparticle demonstrates a promising future as a novel anode material with high capacity in lithium-ion batteries.

Supplementary Materials: The following are available online at <http://www.mdpi.com/2076-3417/8/8/1245/s1>, Figure S1: Galvanostatic charge/discharge profiles SiO_2 electrodes (2 nm, 10 nm, 300 nm, and 3 μm) before and after lithiation; Figure S2: Electrochemical impedance spectroscopy of SiO_2 -4 electrodes before and after prelithiation at the first cycle. Figure S3. The Coulombic efficiency of four $\text{Li}_x\text{Si}/\text{Li}_2\text{O}$ composites. Figure S4. Cycling performance of $\text{Li}_x\text{Si}/\text{Li}_2\text{O}$ -4 composite.

Author Contributions: Y.H., X.L. and Z.L. did the experiment and wrote this work together.

Funding: National Natural Science Foundation of China (Grant No. 21601083), Natural Science Foundation of Jiangsu Province (Grant No. BK20160614), the Fundamental Research Funds for the Central Universities, and Jiangsu Innovative and Entrepreneurial Talent Award.

Acknowledgments: We acknowledge the support from National Laboratory of Solid State Microstructures, Collaborative Innovation Center of Advanced Microstructures, National Natural Science Foundation of China, Natural Science Foundation of Jiangsu Province, the Fundamental Research Funds for the Central Universities, and Jiangsu Innovative and Entrepreneurial Talent Award.

Conflicts of Interest: The authors declare no conflicts of interest.

References

1. Goodenough, J.B. Evolution of strategies for modern rechargeable batteries. *Acc. Chem. Res.* **2012**, *46*, 1053–1061. [[CrossRef](#)] [[PubMed](#)]
2. Chu, S.; Majumdar, A. Opportunities and challenges for a sustainable energy future. *Nature* **2012**, *488*, 294–303. [[CrossRef](#)] [[PubMed](#)]
3. Ji, L.; Lin, Z.; Alcoutlabi, M.; Zhang, X. Recent developments in nanostructured anode materials for rechargeable lithium-ion batteries. *Energy Environ. Sci.* **2011**, *4*, 2682–2699. [[CrossRef](#)]
4. Guo, B.; Shu, J.; Wang, Z.; Yang, H.; Shi, L.; Liu, Y.; Chen, L. Electrochemical reduction of nano- SiO_2 in hard carbon as anode material for lithium ion batteries. *Electrochem. Commun.* **2008**, *10*, 1876–1878. [[CrossRef](#)]

5. Miyachi, M.; Yamamoto, H.; Kawai, H.; Ohta, T.; Shirakata, M. Analysis of SiO Anodes for Lithium-Ion Batteries. *J. Electrochem. Soc.* **2005**, *152*, A2089–A2091. [[CrossRef](#)]
6. Zuniga, L.; Agubra, V.A.; Flores, D.; Campos, H.; Villareal, J.; Alcoutlabi, M. Multichannel hollow structure for improved electrochemical performance of TiO₂/Carbon composite nanofibers as anodes for lithium ion batteries. *J. Alloy. Compd.* **2016**, *686*, 733–743. [[CrossRef](#)]
7. Agubra, V.A.; Zuniga, L.; Flores, D.; Villareal, J.; Alcoutlabi, M. Composite Nanofibers as Advanced Materials for Li-ion, Li-O₂ and Li-S Batteries. *Electrochim. Acta* **2016**, *192*, 529–550. [[CrossRef](#)]
8. Sun, Q.; Zhang, B.; Fu, Z.-W. Lithium electrochemistry of SiO₂ thin film electrode for lithium-ion batteries. *Appl. Surf. Sci.* **2008**, *254*, 3774–3779. [[CrossRef](#)]
9. Nguyen, C.C.; Choi, H.; Song, S.W. Roles of Oxygen and Interfacial Stabilization in Enhancing the Cycling Ability of Silicon Oxide Anodes for Rechargeable Lithium Batteries. *J. Electrochem. Soc.* **2013**, *160*, A906–A914. [[CrossRef](#)]
10. Sasidharan, M.; Liu, D.; Gunawardhana, N.; Yoshio, M.; Nakashima, K. Synthesis, characterization and application for lithium-ion rechargeable batteries of hollow silica nanospheres. *J. Mater. Chem.* **2011**, *21*, 13881. [[CrossRef](#)]
11. Li, X.; Dhanabalan, A.; Meng, X.; Gu, L.; Sun, X.; Wang, C. Nanoporous tree-like SiO₂ films fabricated by sol-gel assisted electrostatic spray deposition. *Microporous Mesoporous Mater.* **2012**, *151*, 488–494. [[CrossRef](#)]
12. Cao, X.; Chuan, X.; Li, S.; Huang, D.; Cao, G. Hollow Silica Spheres Embedded in a Porous Carbon Matrix and Its Superior Performance as the Anode for Lithium-Ion Batteries. *Part. Part. Syst. Charact.* **2016**, *33*, 110–117. [[CrossRef](#)]
13. Yan, N.; Wang, F.; Zhong, H.; Li, Y.; Wang, Y.; Hu, L.; Chen, Q. Hollow porous SiO₂ nanocubes towards high-performance anodes for lithium-ion batteries. *Sci. Rep.* **2013**, *3*, 1568. [[CrossRef](#)] [[PubMed](#)]
14. Favors, Z.; Wang, W.; Bay, H.H.; George, A.; Ozkan, M.; Ozkan, C.S. Stable cycling of SiO₂ nanotubes as high-performance anodes for lithium-ion batteries. *Sci. Rep.* **2014**, *4*, 4605. [[CrossRef](#)] [[PubMed](#)]
15. Wang, H.; Wu, P.; Shi, H.; Tang, W.; Tang, Y.; Zhou, Y.; She, P.; Lu, T. Hollow porous silicon oxide nanobelts for high-performance lithium storage. *J. Power Sources* **2015**, *274*, 951–956. [[CrossRef](#)]
16. Xu, Q.; Li, J.-Y.; Sun, J.-K.; Yin, Y.-X.; Wan, L.-J.; Guo, Y.-G. Watermelon-Inspired Si/C Microspheres with Hierarchical Buffer Structures for Densely Compacted Lithium-Ion Battery Anodes. *Adv. Energy Mater.* **2017**, *7*, 1601481. [[CrossRef](#)]
17. Lin, D.; Lu, Z.; Hsu, P.-C.; Lee, H.R.; Liu, N.; Zhao, J.; Wang, H.; Liu, C.; Cui, Y. A high tap density secondary silicon particle anode fabricated by scalable mechanical pressing for lithium-ion batteries. *Energy Environ. Sci.* **2015**, *8*, 2371–2376. [[CrossRef](#)]
18. Sim, S.; Oh, P.; Park, S.; Cho, J. Critical thickness of SiO₂ coating layer on core@shell bulk@nanowire Si anode materials for Li-ion batteries. *Adv. Mater.* **2013**, *25*, 4498–4503. [[CrossRef](#)] [[PubMed](#)]
19. Wang, H.; Wu, P.; Qu, M.; Si, L.; Tang, Y.; Zhou, Y.; Lu, T. Highly Reversible and Fast Lithium Storage in Graphene-Wrapped SiO₂ Nanotube Network. *ChemElectroChem* **2015**, *2*, 508–511. [[CrossRef](#)]
20. Aravindan, V.; Lee, Y.-S.; Madhavi, S. Best Practices for Mitigating Irreversible Capacity Loss of Negative Electrodes in Li-Ion Batteries. *Adv. Energy Mater.* **2017**, *7*, 1602607. [[CrossRef](#)]
21. Cloud, J.E.; Wang, Y.; Li, X.; Yoder, T.S.; Yang, Y.; Yang, Y. Lithium silicide nanocrystals: Synthesis, chemical stability, thermal stability, and carbon encapsulation. *Inorg. Chem.* **2014**, *53*, 11289–11297. [[CrossRef](#)] [[PubMed](#)]
22. Wang, J.; Luo, H.; Liu, Y.; He, Y.; Fan, F.; Zhang, Z.; Mao, S.X.; Wang, C.; Zhu, T. Tuning the Outward to Inward Swelling in Lithiated Silicon Nanotubes via Surface Oxide Coating. *Nano Lett.* **2016**, *16*, 5815–5822. [[CrossRef](#)] [[PubMed](#)]
23. Zhao, J.; Lu, Z.; Wang, H.; Liu, W.; Lee, H.W.; Yan, K.; Zhuo, D.; Lin, D.; Liu, N.; Cui, Y. Artificial Solid Electrolyte Interphase-Protected Li_xSi Nanoparticles: An Efficient and Stable Prelithiation Reagent for Lithium-Ion Batteries. *J. Am. Chem. Soc.* **2015**, *137*, 8372–8375. [[CrossRef](#)] [[PubMed](#)]
24. Zhao, J.; Sun, J.; Pei, A.; Zhou, G.; Yan, K.; Liu, Y.; Lin, D.; Cui, Y. A general prelithiation approach for group IV elements and corresponding oxides. *Energy Storage Mater.* **2018**, *10*, 275–281. [[CrossRef](#)]
25. Forney, M.W.; Ganter, M.J.; Staub, J.W.; Ridgley, R.D.; Landi, B.J. Prelithiation of silicon-carbon nanotube anodes for lithium ion batteries by stabilized lithium metal powder (SLMP). *Nano Lett.* **2013**, *13*, 4158–4163. [[CrossRef](#)] [[PubMed](#)]

26. Iwamura, S.; Nishihara, H.; Ono, Y.; Morito, H.; Yamane, H.; Nara, H.; Osaka, T.; Kyotani, T. Li-rich Li-Si alloy as a lithium-containing negative electrode material towards high energy lithium-ion batteries. *Sci. Rep.* **2015**, *5*, 8085. [[CrossRef](#)] [[PubMed](#)]
27. Kim, H.J.; Choi, S.; Lee, S.J.; Seo, M.W.; Lee, J.G.; Deniz, E.; Lee, Y.J.; Kim, E.K.; Choi, J.W. Controlled Prelithiation of Silicon Monoxide for High Performance Lithium-Ion Rechargeable Full Cells. *Nano Lett.* **2016**, *16*, 282–288. [[CrossRef](#)] [[PubMed](#)]
28. Li, X.; Kersey-Bronec, F.E.; Ke, J.; Cloud, J.E.; Wang, Y.; Ngo, C.; Pylypenko, S.; Yang, Y. Study of Lithium Silicide Nanoparticles as Anode Materials for Advanced Lithium Ion Batteries. *ACS Appl. Mater. Interfaces* **2017**, *9*, 16071–16080. [[CrossRef](#)] [[PubMed](#)]
29. Sun, Y.; Lee, H.W.; Zheng, G.; Seh, Z.W.; Sun, J.; Li, Y.; Cui, Y. In Situ Chemical Synthesis of Lithium Fluoride/Metal Nanocomposite for High Capacity Prelithiation of Cathodes. *Nano Lett.* **2016**, *16*, 1497–1501. [[CrossRef](#)] [[PubMed](#)]
30. Wang, Z.; Fu, Y.; Zhang, Z.; Yuan, S.; Amine, K.; Battaglia, V.; Liu, G. Application of Stabilized Lithium Metal Powder (SLMP[®]) in graphite anode—A high efficient prelithiation method for lithium-ion batteries. *J. Power Sources* **2014**, *260*, 57–61. [[CrossRef](#)]
31. Zhao, J.; Lee, H.W.; Sun, J.; Yan, K.; Liu, Y.; Liu, W.; Lu, Z.; Lin, D.; Zhou, G.; Cui, Y. Metallurgically lithiated SiO_x anode with high capacity and ambient air compatibility. *Proc. Natl. Acad. Sci. USA* **2016**, *113*, 7408–7413. [[CrossRef](#)] [[PubMed](#)]
32. Zhao, J.; Lu, Z.; Liu, N.; Lee, H.W.; McDowell, M.T.; Cui, Y. Dry-air-stable lithium silicide-lithium oxide core-shell nanoparticles as high-capacity prelithiation reagents. *Nat. Commun.* **2014**, *5*, 5088. [[CrossRef](#)] [[PubMed](#)]
33. Zhao, J.; Zhou, G.; Yan, K.; Xie, J.; Li, Y.; Liao, L.; Jin, Y.; Liu, K.; Hsu, P.C.; Wang, J.; et al. Air-stable and freestanding lithium alloy/graphene foil as an alternative to lithium metal anodes. *Nat. Nanotechnol.* **2017**, *12*, 993–999. [[CrossRef](#)] [[PubMed](#)]
34. Wang, C.; Han, Y.; Li, S.; Chen, T.; Yu, J.; Lu, Z. Thermal Lithiated-TiO₂: A Robust and Electron-Conducting Protection Layer for Li-Si Alloy Anode. *ACS Appl. Mater. Interfaces* **2018**, *10*, 12750–12758. [[CrossRef](#)] [[PubMed](#)]
35. Lepoivre, F.L.D.; Tarascon, J.M. Electrochemical Activation of Silica for Enhanced Performances of Si-Based Electrodes. *J. Electrochem. Soc.* **2016**, *163*, A2791–A2796. [[CrossRef](#)]
36. Jarvis, C.R.; Lain, M.J.; Yakovleva, M.V.; Gao, Y. A prelithiated carbon anode for lithium-ion battery applications. *J. Power Sources* **2006**, *162*, 800–802. [[CrossRef](#)]
37. Wang, L.; Fu, Y.; Battaglia, V.S.; Liu, G. SBR–PVDF based binder for the application of SLMP in graphite anodes. *RSC Adv.* **2013**, *3*, 15022. [[CrossRef](#)]



© 2018 by the authors. Licensee MDPI, Basel, Switzerland. This article is an open access article distributed under the terms and conditions of the Creative Commons Attribution (CC BY) license (<http://creativecommons.org/licenses/by/4.0/>).